

Compression and stretching of ring vortexin a bulk nonlinear medium

Xian-Jing Lai(来娴静), Xiao-Ou Cai(蔡晓鸥), Ya-Bin Shao(邵雅斌), and Yue-Yue Wang(王悦悦)

Citation: Chin. Phys. B, 2024, 33 (**2**): 020506. DOI: 10.1088/1674-1056/ad01a0
Journal homepage: http://cpb.iphy.ac.cn; http://iopscience.iop.org/cpb

What follows is a list of articles you may be interested in

Characteristic analysis of 5D symmetric Hamiltonian conservative hyperchaotic system with hidden multiple stability

Li-Lian Huang(黄丽莲), Yan-Hao Ma(马衍昊), and Chuang Li(李创)
Chin. Phys. B, 2024, 33 (**1**): 010503. DOI: 10.1088/1674-1056/acf9e7

Distributed dynamic event-based finite-time dissipative synchronization control for semi-Markov switched fuzzy cyber-physical systems against random packet losses

Xiru Wu(伍锡如), Yuchong Zhang(张煜翀), Tiantian Zhang(张畑畑), and Binlei Zhang(张斌磊)
Chin. Phys. B, 2023, 32 (**10**): 100506. DOI: 10.1088/1674-1056/acb91b

Unstable periodic orbits analysis in the Qi system

Lian Jia(贾莲), Chengwei Dong(董成伟), Hantao Li(李瀚涛), and Xiaohong Sui(眭晓红)
Chin. Phys. B, 2023, 32 (**4**): 040502. DOI: 10.1088/1674-1056/aca9c3

Localized nonlinear waves in a myelinated nerve fiber with self-excitable membrane

Nkeh Oma Nfor, Patrick Guemkam Ghomsi, and Francois Marie Moukam Kakmeni
Chin. Phys. B, 2023, 32 (**2**): 020504. DOI: 10.1088/1674-1056/ac720d

Dynamics of high-frequency modulated waves in a nonlinear dissipative continuous bi-inductance network

S M Ngounou and F B Pelap
Chin. Phys. B, 2021, 30 (**6**): 060504. DOI: 10.1088/1674-1056/abd751

Compression and stretching of ring vortex in a bulk nonlinear medium

Xian-Jing Lai(来娴静)[1,†], Xiao-Ou Cai(蔡晓鸥)[1,‡], Ya-Bin Shao(邵雅斌)[1], and Yue-Yue Wang(王悦悦)[2]

[1] *Department of Basic Science, Zhejiang Shuren University, Hangzhou* 310015, *China*
[2] *School of Sciences, Zhejiang A&F University, Hangzhou* 311300, *China*

(Received 13 July 2023; revised manuscript received 8 October 2023; accepted manuscript online 10 October 2023)

We explore the nonlinear gain coupled Schrödinger system through the utilization of the variables separation method and ansatz technique. By employing these approaches, we generate hierarchies of explicit dissipative vector vortices (DVVs) that possess diverse vorticity values. Numerous fundamental characteristics of the DVVs are examined, encompassing amplitude profiles, energy fluxes, parameter effects, as well as linear and dynamic stability.

Keywords: vector optical vortices, dissipative, nonlinear gain

PACS: 05.45.Yv, 03.75.Lm, 42.65.Tg **DOI:** 10.1088/1674-1056/ad01a0

1. Introduction

Dissipative solitons, found abundantly in nature across diverse branches of natural science, emerge as a result of the delicate equilibrium between dispersion, nonlinearity, gain, and loss. They serve as an excellent platform for investigating nonlinear optical dynamics in multiple physical disciplines, including nonlinear optics, fluid dynamics, plasma physics, complex networks, and molecular biology.[1–6] Among dissipative solitons, the dissipative vortex[7–9] is noteworthy. Dissipative vortex structures with nonzero angular momenta have counterparts in nature, such as tornadoes. Vortex solitons self-organize around the zero-strength topological singularity at their center and are characterized by topological charges.[10–14] A dissipative vortex with a fundamental vorticity spontaneously breaks axial symmetry due to modulation instability and can either evolve into a stable rotating ellipsoidal soliton or fragment into filaments. It is generally believed that vortex structures with high topological charges are unstable because modulation instability increases with higher vorticity. Indeed, for higher vorticity, the vortex radius enlarges, intensifying modulation instability and leading to the filamentary disruption of the vortex.

In addition to scalar vortices, many nonlinear systems support vector vortices. The formation of vector vortices is based on the fact that vortices are modes that exist in single-component two-dimensional media. Extending the concept of vortices to two components is both natural and intriguing. Compared to single vortex beams, vector vortex beams offer greater flexibility in beam manipulation, allowing for the creation of more unique beam structures to meet various application requirements. The vector vortex beam, renowned for its vector polarization and helical phase, has been a subject of extensive research due to its potential applications in high-resolution imaging, data storage, micromanipulation, molecular orientation research, and 3D beam shaping. In pursuit of these applications, numerous remarkable technologies have been proposed to generate vector vortex beams; however, the creation of novel vector vortex beams remains a significant challenge.[15–18] Despite the availability of numerous numerical investigations, the analytical analysis concerning the formation of vector vortex solitons remains relatively limited.

Research of multicomponent nonlinear systems, involving evolutionary partial differential equations, has gained significant attention in recent years, especially in the fields of optics and atomic physics where multicomponent structures are commonly observed. To thoroughly analyze the propagation of solitons in such systems, researchers often turn to the nonlinear Schrödinger equation, which effectively captures the simultaneous evolution of multiple classes of solitons.[19–21] Among these equations, the coupled nonlinear Schrödinger (CNLS) equation stands out, drawing considerable interest in the realms of mathematics and physics. This is due to its ability to support two-component fundamental modes under various optical conditions.[22–26] These equations find widespread application across various branches of physics, including electromagnetics, hydrodynamics, zero-temperature Bose–Einstein condensates, and plasma physics. In particular, within the field of optics, CNLS systems are frequently employed to describe the propagation of light in birefringent fibers. Their versatility in modeling cross-phase and self-phase modulation makes them indispensable tools for understanding complex optical phenomena.

Typically, vector solitons within two-dimensional homogeneous Kerr-type nonlinear media exhibit inherent instability

[†]Corresponding author. E-mail: laixianjing@163.com
[‡]Corresponding author. E-mail: Cai.xo@163.com

© 2024 Chinese Physical Society and IOP Publishing Ltd

and are susceptible to collapse. However, specific settings, such as spatial modulation nonlinearity,[11,13] can enhance the stability and extend the propagation distance of solitons. In these cases, the fundamental soliton exhibits remarkable stability despite the absence of homogeneity. It is natural to anticipate that the introduction of spatially varying nonlinearity would confer a beneficial influence on the stability of vector systems featuring vortex components. This leads to a natural question: Can spatially varying nonlinearity in a dissipative optical system with nonlinear gain excite vector vortex structures? and if so, how do they evolve? Exploring these questions is both practically significant and the main focus of this study.

In this paper, we present an efficient analytical scheme for the CNLS equation, considering the simultaneous existence of spatial modulation potential energy, nonlinear and linear gain. We delve into the fascinating realm of generating DVVs within this framework, offering a comprehensive exploration of their key attributes. Our analysis delves into how various parameters influence the structural features and energy dynamics of these DVVs. Furthermore, we employ rigorous linear stability analysis to assess the stability of these solitons, providing insights into their robustness. This work addresses several challenges by employing variable separation techniques[27–29] to simplify the problem, resulting in analytical solutions for DVVs in CNLS systems with spatial modulation nonlinearity. The DVVs structures we uncover, expressed in cylindrical coordinates, resemble higher-order beams observed in cylindrical waveguides, such as Laguerre–Gaussian, Whitaker–Gaussian, or Bessel–Gaussian modes, featuring the utilization of Bessel–Gaussian or Bessel–Hyperbolic functions. This comprehensive study allows us to gain a profound understanding of how the effective radius and energy flow of the vortex core evolve with varying parameters. Additionally, our theoretical stability analysis offers valuable insights into the resilience of DVVs under different propagation constants, enhancing our ability to predict their stability.

2. Analytical vector vortices

Presuming that the vector field has N irrelevant scalar components coupled by nonlinear effects, the system can be expressed as

$$\mathrm{i}\frac{\mathrm{d}\psi_j}{\mathrm{d}z}+\frac{\beta}{2}\nabla^2\psi_j+\left(\tilde{\gamma}+\mathrm{i}\frac{\tilde{\alpha}}{2}\right)\sum_{j=1}^{N}|\psi_j|^2\psi_j+V\psi_j=\mathrm{i}\frac{g_0}{2}\psi_j, \tag{1}$$

where ψ_j are the slowly varying envelopes in the presence of transverse modulation $V\equiv V(x,y)$ and propagation distance z. The influence of the function $V(x,y)$ opposes the impact of nonlinearity, resulting in its attenuation. To find solutions for Eq. (1), we define the complex fields ψ_j as

$$\psi_j=\eta\Phi_j, \tag{2}$$

with η being a real function of z. One can find the coupled averaged equations for the Φ_j as follows:

$$\mathrm{i}\frac{\mathrm{d}\Phi_j}{\mathrm{d}z}+\frac{\beta}{2}\nabla^2\Phi_j+\left(\gamma+\mathrm{i}\frac{\alpha}{2}\right)\sum_{j=1}^{N}|\Phi_j|^2\Phi_j+V\Phi_j=0, \tag{3}$$

where

$$\alpha=\tilde{\alpha}\eta^2,\quad \gamma=\tilde{\gamma}\eta^2, \tag{4}$$

$$\eta=\eta_0\exp\left[\int_0^z\frac{1}{2}g_0(z')\mathrm{d}z'\right]. \tag{5}$$

One assumes that Eq. (2) possesses the following ansatz:

$$\Phi_j=P(r)\varphi_j(\theta)\exp[\mathrm{i}\mu z-\mathrm{i}H\ln(P(r))] \tag{6}$$

with partially separated variables, where P and φ_j are the amplitude profile and the azimuthal part, respectively, $r^2=x^2+y^2$ is the radial distance, μ is propagation constant, and $\theta=\tan^{-1}(y/x)$, which is the polar angle. Substituting Eq. (6) into Eq. (3), one obtains a set of conditions on the coefficients and parameters:

$$\beta r^2HP\frac{\mathrm{d}^2P}{\mathrm{d}r^2}+r\left(P^4r\alpha\sum_{j=1}^{N}|\varphi_j|^2+H\beta r\left(\frac{\mathrm{d}P}{\mathrm{d}r}\right)^2+H\beta P\frac{\mathrm{d}P}{\mathrm{d}r}\right)=0, \tag{7}$$

$$\varphi_j\beta r^2P\frac{\mathrm{d}^2P}{\mathrm{d}r^2}+P^2\beta\frac{\mathrm{d}^2\varphi_j}{\mathrm{d}\theta^2}+r\varphi_j\Big[-H^2\beta r\left(\frac{\mathrm{d}P}{\mathrm{d}r}\right)^2+\beta P\frac{\mathrm{d}P}{\mathrm{d}r}$$
$$+2P^2r\left(P^2\gamma\sum_{j=1}^{N}|\varphi_j|^2+V+\mu\right)\Big]=0. \tag{8}$$

Considering the self-consistency condition

$$\sum_{j=1}^{N}|\varphi_j|^2=1, \tag{9}$$

the azimuthal part of the solution can be written as

$$\varphi_j=a_j\cos(m\theta)+b_j\sin(m\theta), \tag{10}$$

$$-\frac{\mathrm{d}^2\varphi_j}{d\theta^2}=m^2\varphi_j. \tag{11}$$

The value of m is assigned as the topological charge. For our analysis, we specifically focus on the scenario where there are two components, denoted by $N=2$, thereby ensuring a two-component case:

$$a_1=\sqrt{-a_2^2+1},\quad b_1=\mathrm{i}\sqrt{d^2p^2-d^2+1},\quad b_2=\mathrm{i}d\sqrt{1-p^2} \tag{12}$$

with the limitation factors

$$a_2^2<1,\quad d^2<\frac{1}{1-p^2}. \tag{13}$$

By setting the modulation depth p to 0 and 1, we construct vector multipole and vortex solitons, respectively. The amplitude profile P in Eq. (6) satisfies

$$2P^4\gamma r^2+P^4\alpha r^2H^{-1}+2P^2Vr^2+2P\beta r^2\frac{\mathrm{d}^2P}{\mathrm{d}r^2}$$

$$+2P^2\mu r^2+2P\beta r\frac{\mathrm{d}P}{\mathrm{d}r}-P^2m^2\beta=0. \tag{14}$$

Introducing the following ansatz for the stationary fields:

$$P=\rho(r)U(R) \tag{15}$$

with

$$R=\exp\Big[\int_0^r\frac{1}{r'\rho(r')^2}\mathrm{d}r'\Big], \tag{16}$$

we have

$$2V\rho^4r^2+2\rho^3\beta r^2\frac{\mathrm{d}^2\rho}{\mathrm{d}r^2}-\rho^4\beta m^2+2\rho^4\mu r^2$$
$$+2\rho^3\beta r\frac{\mathrm{d}\rho}{\mathrm{d}r}=2\beta E. \tag{17}$$

When the external potential takes

$$V=\frac{\beta(-kr^4\rho^4+E)}{\rho^4r^2}, \tag{18}$$

the self-consistency condition is satisfied when the nonlinear and coupling coefficients in Eq. (3) meet the following criteria:

$$\gamma=\frac{-\alpha r^2\rho^6+2H\beta g}{2(H\rho^6r^2)}, \tag{19}$$

with U satisfying for solving the ordinary differential equation

$$\frac{\mathrm{d}^2U}{\mathrm{d}R^2}+EU(R)+gU(R)^3=0, \tag{20}$$

and the quantity ρ fulfills

$$-kr^2\rho+\rho\sigma+\frac{\mathrm{d}^2\rho}{\mathrm{d}r^2}-\rho\frac{\tilde{S}^2}{r^2}+\frac{1}{r}\frac{\mathrm{d}\rho}{\mathrm{d}r}=0, \tag{21}$$

where

$$\tilde{S}=\frac{\sqrt{2}}{2}m,\quad \sigma=\frac{\mu}{\beta}. \tag{22}$$

Applying the aforementioned procedure leads to the reduction of the coupled NLSE (1) to a solvable stationary nonlinear Schrödinger equation (20) alongside Eq. (21).

Equations (20) and (21) admit the following solutions:

$$U=\frac{s\sqrt{\mathrm{CN}[K(s)(2\varepsilon jR-1),s]^2}}{\sqrt{1-s^2\mathrm{SN}[K(s)(2\varepsilon jR-1),s]^2}} \tag{23}$$

with

$$E=4\varepsilon^2j^2K(s)^2(s^2+1),\ \ g=-8\varepsilon^2j^2K(s)^2, \tag{24}$$
$$\rho=r^{-1}[\kappa_1M_{\iota_1,\iota_2}(\nu)+\kappa_2W_{\iota_1,\iota_2}(\nu)], \tag{25}$$

where CN$[\cdot]$ and SN$[\cdot]$ are Jacobi elliptic functions, and s $(0\le s\le 1)$ is the modulus, $K(\cdot)$ is elliptic integral of the first kind. The functions $M_{\iota_1,\iota_2}(\nu)$ and $W_{\iota_1,\iota_2}(\nu)$ correspond to the Whittaker functions, with $\iota_1=\frac{1}{4}k^{-1/2}\sigma$, $\iota_2=\frac{\tilde{S}}{2}$, and $\nu=k^{-1/2}r^2$. The constants κ_1 and κ_2 are arbitrary. The multipole solitons exhibit a specific number of azimuthal lobes, determined by the topological charge m as $2m$, and the number of layers is determined by the index value j. These solitons encompass a range of topological charges from 1 to 5, corresponding to dipole, quadrupole, hexapole, octopole, and dodecagon solitons. The limit values represent multipole vector solitons ($p=0$) and vector vortex solitons ($p=1$). The parameter $\varepsilon_{r\to\infty}=R^{-1}$ in Eq. (23) ensures that the boundary conditions $U_{r=0}=U_{r=\infty}=0$ are satisfied. It is worth mentioning that the spatially varying strength of nonlinearity is confined within certain bounds, and the integration in $V(r)$ converges, as indicated in Ref. [15]. Therefore, the expressions for $V(r)$ and $\gamma(r)$ impose certain conditions: ρ must not change sign and exhibit behavior as $r^{-\varpi}$ with $\varpi\ge 3^{-1}$ as r approaches zero, while ρ diverges as r tends to infinity. These restrictions imply that $\kappa_1\kappa_2>0$ and $\sigma<2(1+\tilde{S})k^{-1/2}$ in Eq. (10), resulting in $\mu<4(1+\tilde{S})k^{-1/2}$. Consequently, the cubic nonlinearity is defocusing ($\gamma<0$) in this case.

A breakthrough methodology arises from the establishment of a direct mapping between Eqs. (1) and (20), enabling the systematic exploration of numerous precise "soliton islands" amidst an extensive realm of solitary waves. By leveraging a variety of U forms, the solutions of Eq. (20) can be utilized to derive solutions for Eq. (1). By transforming Eq. (20) into well-known Schrödinger equations, abundant solutions for Eq. (20) can be generated. Therefore, utilizing Eqs. (2), (6), (15), (23), and (25), a variety of spatially localized stationary exact solutions for Eq. (1) can be derived:

$$\psi_j(r,\theta,z)=\eta_0\exp\Big[\int_0^z\frac{1}{2}g_0(z')\mathrm{d}z'\Big]\rho U[a_j\cos(m\theta)$$
$$+b_j\sin(m\theta)]\exp[\mathrm{i}\mu z-\mathrm{i}H\ln(\rho U)]. \tag{26}$$

Figures 1 and 2 illustrate typical examples of vector vortex mode compositions with different values of m and j, clearly demonstrating their vortex characteristics. Vortex solitons with varying m exhibit phase dislocations, where the phase increases by $2m\pi$ around these dislocations. For a fixed j, the structure expands radially as m increases. In a similar manner, when m is held to be constant, the "petals" within the outermost layer progressively expand radially with increasing j. The solution structure changes as its parameters are varied. Figure 3 demonstrates that $|\psi_1|$ undergoes a transition from a ring-shaped distribution to a multipole, and then undergoes rotation as d changes. The solution structure undergoes changes earlier with larger modulation depth p, resulting in ring-shaped distributions when $h<0.5$. The phase distribution is similar to Fig. 1 and is not drawn to avoid repetition.

Energy balance and energy fluxes hold significant importance in dissipative structures. The Poynting vector serves as a fundamental metric for energy transfer, denoting the density of energy flux or the rate of electromagnetic energy transfer per unit area. In the context of the paraxial approximation utilized

in this study, the dimensionless form of the transverse Poynting vector, when averaged over the optical period, is expressed as

$$S_\perp = \mathrm{Im}(\Phi_j^* \nabla_\perp \Phi_j), \tag{27}$$

where Φ_j is given by Eq. (6). By examining the sign of the divergence of the transverse Poynting vector, one can distinguish between energy sinks and energy sources within the transverse section, thereby enabling the separation of domains with contrasting energy characteristics:

$$\nabla_\perp S_\perp = \frac{\partial S_x}{\partial x} + \frac{\partial S_y}{\partial y} = \mathrm{Im}(\Phi_j^* \nabla_\perp^2 \Phi_j). \tag{28}$$

Analyzing the curl or vorticity of the Poynting vector allows for the identification of energy flow rotation. Within our particular geometry, the Poynting vector is exclusively composed of a longitudinal component:

$$\nabla_\perp \times S_\perp = 2\mathrm{Im}[(\partial_x \Phi_i^*)(\partial_y \Phi_i)] e_z, \tag{29}$$

where * denotes complex conjugation, and e_z represents the unit vector along the z-axis. The vorticity direction, no matter whether it is parallel or antiparallel to e_z, depends on the sign of the right-hand side of Eq. (12). Figure 4 displays the radial dependence of energetic characteristics, with both components having the same radial distribution.

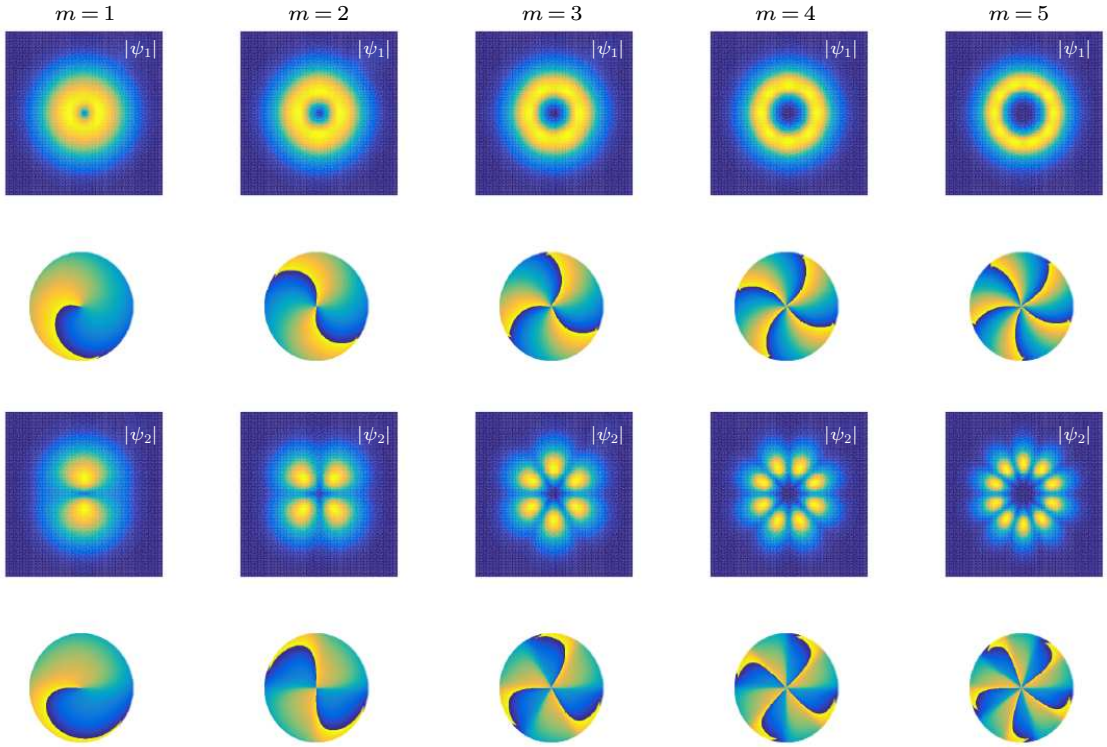


Fig. 1. Example of DVVs of Eq. (26) for different topological charge m with $j = 1$, $p = 0.99$, $g_0 = 0$, $\mu = 0.12$, $\beta = d = 0.5$, $\eta_0 = -H = \kappa_1 = \kappa_2 = 1$, $k = s = 0.01$, $\alpha = -0.2$, and $a_2 = 1 - p^2$. Intensities and phase profiles are shown at $z = 0$.

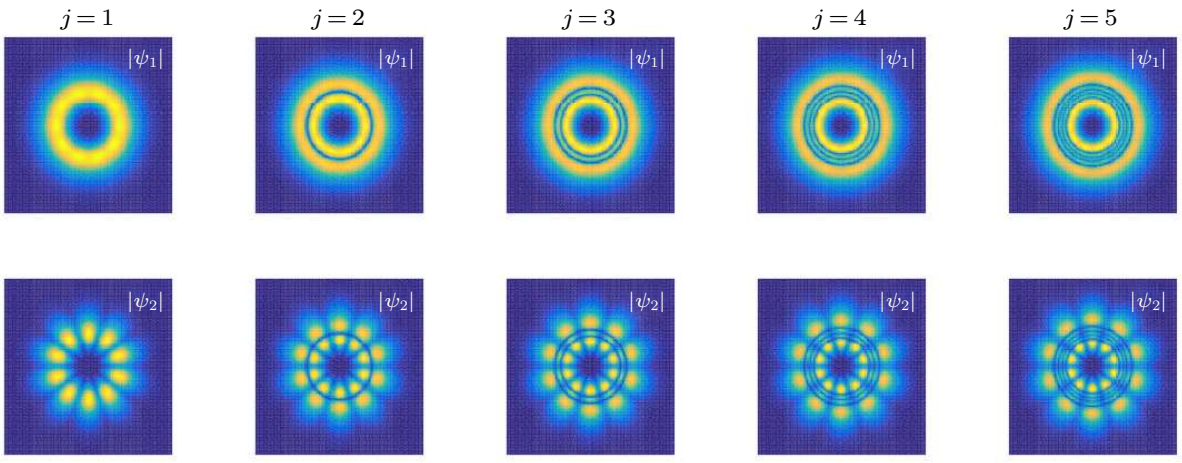


Fig. 2. Example of DVVs of Eq. (26) with topological charge $j = 1,2,3,4,5$, $m = 5$. Other relative parameters are the same as those in Fig. 1. Intensities are shown at $z = 0$.

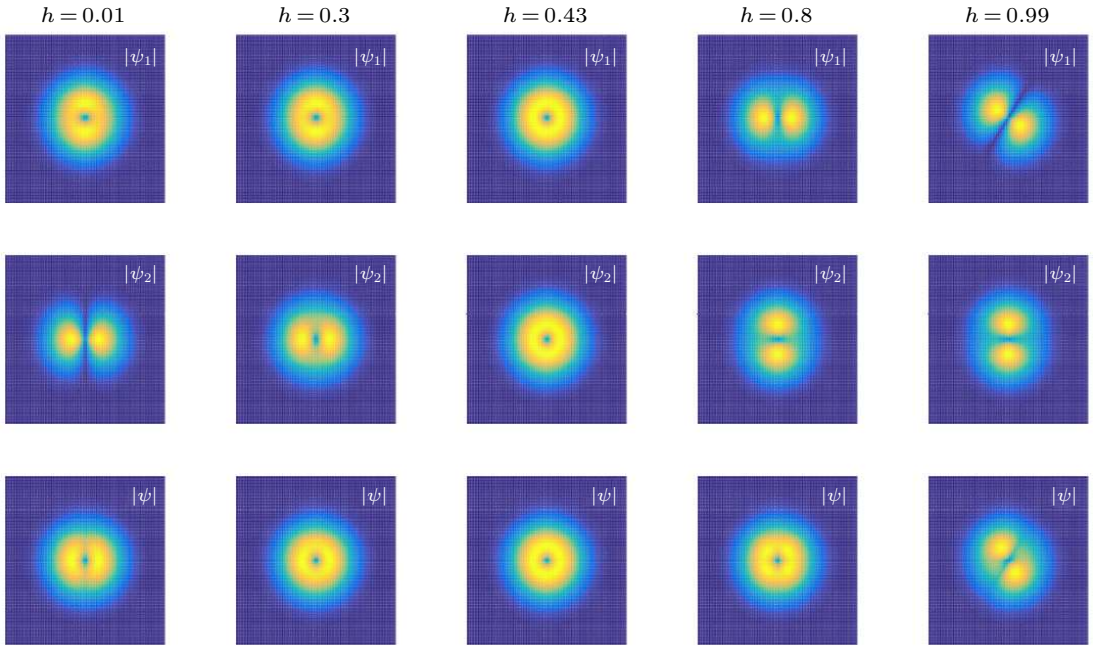


Fig. 3. Two components of DVVs of Eq. (26) orthogonally arrange in first row and second row, and incoherently superpose to form total quantity $|\psi|^2=|\psi_1|^2+|\psi_2|^2$ at $z=0$ for different h. The parameters are $m=1$, $j=1$, $p=0.5$, $s=0.1$, $d=h/(1-p^2)$, $a_2=0.5$. Other relative parameters are the same as those in Fig. 1.

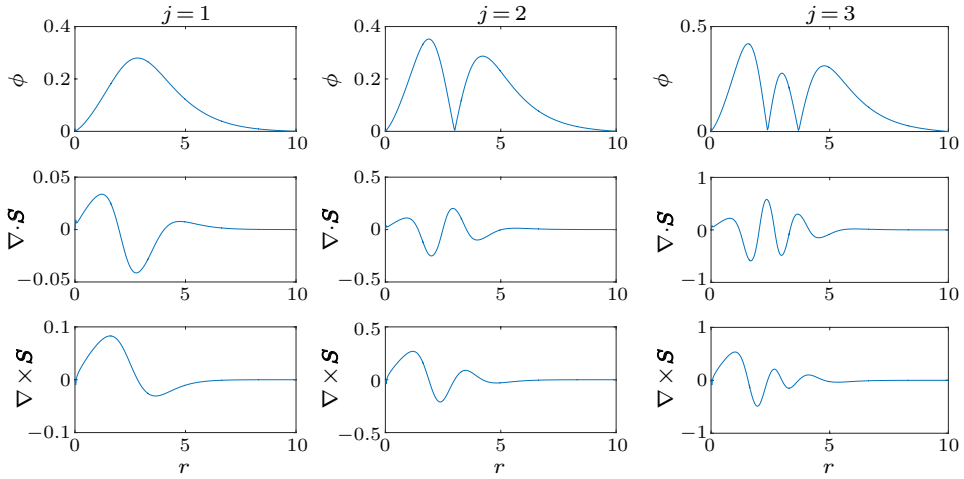


Fig. 4. Radial dependencies of energetic characteristics: intensity (top) and divergence (middle) and vorticity (bottom) of the Poynting vector. The parameters are $m=2$, $p=0.5$, $s=0.5$, $d=0.2$, $a_2=0.5$. Other relative parameters are the same as those in Fig. 1.

3. Linear stability analysis of the DVVs

To comprehensively investigate the dynamics of the DVVs featuring diverse topological charges, it is essential to analyze the linear eigenvalue spectra of the corresponding linear system. In this section, we employ linear stability analysis to illustrate and examine the evolution of the above-acquired DVVs. To evaluate the dynamic stability of them, we introduce perturbations to the nonlinear modes using the following expression:

$$\begin{aligned}\psi_j(r,\theta,z)=&[Q(r)+R_j(r)\phi_j(\theta)\exp(\lambda z)\\&+P_j^*(r)\phi_j^*(\theta)\exp(\lambda^* z)]\varphi_j(\theta)\\&\times\exp\Big(-\mathrm{i}\mu z+\frac{1}{2}g_0 z\Big),\quad j=1,2,\end{aligned}\tag{30}$$

where

$$\begin{aligned}\varphi_j(\theta)&=a_j\cos(m\theta)+b_j\sin(m\theta),\\\phi_j(\theta)&=a_j\cos(p\theta)+b_j\sin(p\theta),\end{aligned}\tag{31}$$

and the asterisk symbolizes the complex conjugate, λ denotes the eigenvalue, p (with $p=m,m-1,\ldots,1$) represents the azimuthal perturbation index, R_j and P_j are the perturbations satisfying the conditions $|R_j|\le Q$ and $|P_j|\le Q$, respectively.

$$Q(r)=\eta_0 P(r)\exp[-\mathrm{i}H\ln(P(r))],\tag{32}$$

satisfying

$$\begin{aligned}&\Big[\frac{\beta}{2}\varphi_j\frac{\mathrm{d}^2}{\mathrm{d}r^2}+\frac{\beta\varphi_j}{2r}\frac{\mathrm{d}}{\mathrm{d}r}+\frac{\beta}{2r^2}\frac{\mathrm{d}^2\varphi_j}{\mathrm{d}\theta^2}+\Big(\gamma+\mathrm{i}\frac{\alpha}{2}\Big)\varphi_j\sum_{j=1}^{N}|\varphi_j|^2|Q|^2\\&+(V+\mu)\varphi_j\Big]Q=0,\end{aligned}\tag{33}$$

with

$$\beta r^2 HP\frac{\mathrm{d}^2P}{\mathrm{d}r^2}+r\left(P^4r\alpha+H\beta r\left(\frac{\mathrm{d}P}{\mathrm{d}r}\right)^2+H\beta P\frac{\mathrm{d}P}{\mathrm{d}r}\right)=0. \quad (34)$$

By substituting the perturbed variable ψ_j into Eq. (1) and linearizing it with respect to the unperturbed solution, an eigenvalue problem arises:

$$\begin{aligned}
\lambda R_1 =& [\zeta_1(1)+\omega_1(1)]R_1+\zeta_3(1)P_1+\zeta_2(2)\omega_4R_2\\
&+\zeta_3(2)\omega_4P_2,\\
\lambda P_1 =& -\zeta_3^*(1)R_1-[\zeta_1^*(1)+\omega_2(1)]P_1-\zeta_3^*(2)\omega_4R_2\\
&-\zeta_2^*(2)\omega_4P_2,\\
\lambda R_2 =& \zeta_2(1)\omega_3R_1+\zeta_3(1)\omega_3P_1+[\zeta_1(2)+\omega_1(2)]R_2\\
&+\zeta_3(2)P_2,\\
\lambda P_2 =& -\zeta_3^*(1)\omega_3R_1-\zeta_2^*(1)\omega_3P_1-\zeta_3^*(2)R_2\\
&-[\zeta_1^*(2)+\omega_2(2)]P_2, \qquad (35)\\
\zeta_1(j) =& \frac{\beta}{2}\left(\frac{\mathrm{d}^2}{\mathrm{d}r^2}+\frac{1}{r}\frac{\mathrm{d}}{\mathrm{d}r}\right)+(|\varphi_j|^2+1)F|Q|^2\\
&+\mu-\frac{\beta}{2r^2}(p^2+m^2),\\
\zeta_2(j) =& F|Q|^2|\varphi_j|^2,\ \ \zeta_3(j)=FQ^2|\varphi_j|^2,\\
\omega_1(j) =& \frac{\varphi_{j\theta}\phi_{j\theta}\beta}{\varphi_j\phi_jr^2},\ \ \omega_2(j)=\frac{\varphi_{j\theta}^*\phi_{j\theta}\beta}{\varphi_j^*\phi_jr^2},\\
\omega_3 =& \frac{\phi_1}{\phi_2},\ \ \omega_4=\frac{\phi_2}{\phi_1}, \qquad (36)
\end{aligned}$$

where $(\cdot)_\theta$ stands for derivative of θ, and * stands for complex conjugation.

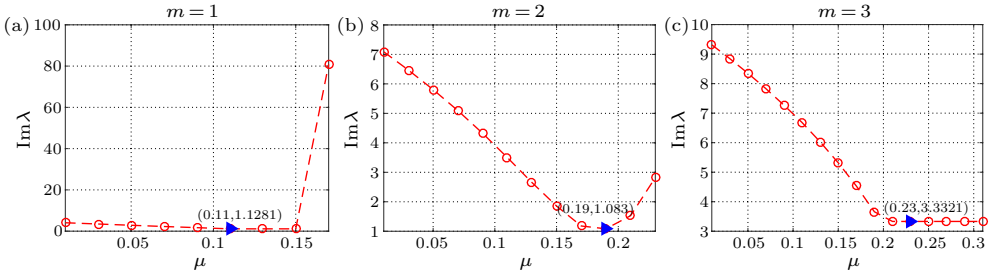


Fig. 5. Growth rate of DVVs of Eq. (26) with different fixed charges $m=1,2,3$ for parameters $j=1$, $p=0.6$, $s=0.6$, $d=0.68$, $a_2=\sqrt{0.3}$. Other relative parameters are the same as those in Fig. 1. The value shown near the arrow is the minimum.

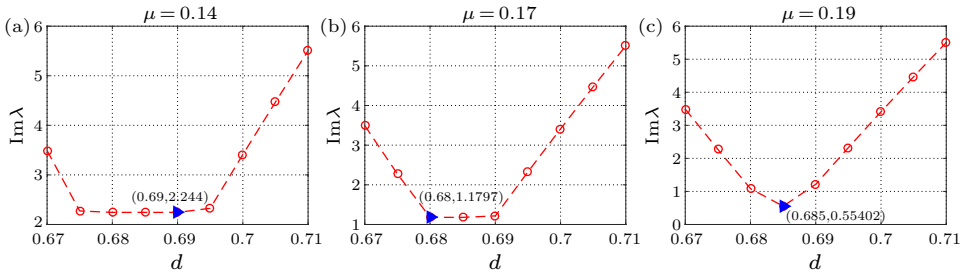


Fig. 6. Growth rate of DVVs of Eq. (26) with different propagation constant μ for topological charge $m=2$. Other relative parameters are the same as those in Fig. 5. The value shown near the arrow is the minimum.

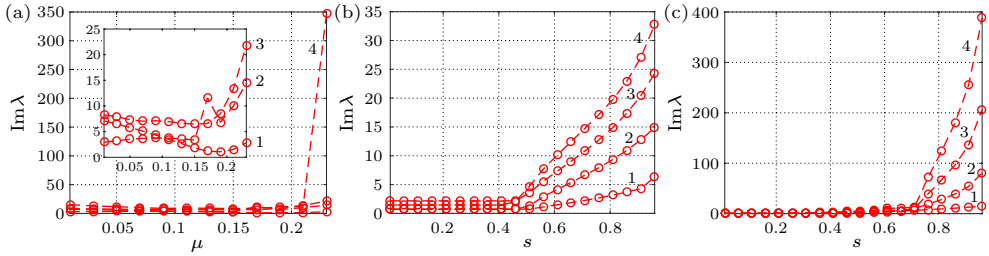


Fig. 7. Growth rate of DVVs of Eq. (26) (a) for different index j with $m=2$, $s=0.6$, $p=0.6$, $d=0.68$, (b) for different topological charge m with $j=1$, $p=0.99$, $d=3.9$, (c) for different index j with $m=2$, $p=0.99$, $d=3.9$ versus related parameters. Other relative parameters are the same as those in Fig. 5.

The parameters are pivotal in determining the linear stability of DVVs. We maintain certain parameters while altering others during our analysis. Figures 1–4 illustrate how μ, s, and d influence eigenvalue spectra, with the blue triangle representing minimum values. For instance, when $s=0.01$, $p=0.01$, and $d=0.1$, the vector vortex adopts a circular shape, resulting in the smallest eigenvalue and the most stable propagation. To minimize the eigenvalue within the given range of μ, we adjust μ to reach a minimum eigenvalue of 1.083 by setting $\mu=0.19$ and fine-tune d to reduce it further to 0.55402 for $d=0.685$. Figure 1 depicts the relationship between the instability growth rate and μ or s for different m and

j values. Larger m values generally yield greater eigenvalues when other parameters remain constant. The impact of j on stability depends on the value of s. For small s, such as $s = 0.1$, the effect of j on linear stability is minimal, resulting in similar stability properties for vector solitons with different j but the same m. Conversely, with a large s, such as $s = 0.6$, the influence of j on the eigenvalue becomes more pronounced. It is essential to note that our research assumes a constant nonlinear gain of $\alpha = -0.2$. For $m \geq 1$, stable vortex solitons are not found. Vortices with lower power levels tend to collapse progressively, while those with higher topological charges become unstable and transform into lower topological charges at higher power levels. This behavior arises from strong interactions between nonlinear internal modes. However, when nonlinear gain is modulated, the stability of the vector vortex solution significantly improves. Stable vortices with higher topological charges, characterized by multiple phase dislocations, maintain their shapes and phases over long distances without distortion. Further exploration of this aspect awaits future research endeavors.

4. Conclusions

In summary, we propose an efficient approach to analyze the CNLS equation with spatial modulation, nonlinearity, and linear gain. We investigate DVVs and their properties in this nonlinear system. By considering two components, we construct DVVs and study their structure and energy flow influenced by parameters. Additionally, we analyze specific DVV structures to understand the impact of parameter changes on the vortex core. We assess soliton stability using linear stability analysis. Challenges addressed include variable separation, obtaining analytical solutions, and predicting stability based on disturbance growth rates.

Acknowledgement

This work was supported by the National Natural Science Foundation of China (Grant Nos. 11705164 and 11874324).

References

[1] Peng J S, Boscolo S, Zhao Z H and Zeng H P 2019 *Sci. Adv.* **5** 1110
[2] Lai X J, Cai X O and Zhang J F 2018 *Commun. Theor. Phys.* **69** 159
[3] Akhmediev N and Ankiewicz A 2008 *Dissipative Solitons: From Optics to Biology and Medicine* (Berlin: Springer) *Lecture Notes in Physics* Vol. 751 p. 1
[4] Renninger W H, Chong A and Wise F W 2008 *Phys. Rev. A* **77** 023814
[5] Grelu P and Akhmediev N 2012 *Nat. Photon.* **6** 84
[6] Rosanov N N and Fedorov S V 2016 *J. Opt.* **18** 074005
[7] Chestnov I, Yulin A, Shelykh I A and Kavokin A 2021 *Phys. Rev. B* **104** 165305
[8] Kochetov B A and Tuz V R 2018 *Phys. Rev. E* **98** 062214
[9] Clerc M G, Gonzalez-Cortes G and Echeverria-Alar S 2022 *Phys. Rev. Res.* **4** L022021
[10] Desyatnikov A, Torner L and Kivshar Y 2005 *Prog. Opt.* **47** 291
[11] Dai C Q, Zhou G Q, Chen R P, Lai X J and Zheng J 2017 *Nonlinear Dyn.* **88** 2629
[12] Minzoni A, Smyth N, Xu Z and Kivshar Y 2009 *Phys. Rev. A* **79** 063808
[13] Tian Q, Wu L, Zhang Y H and Zhang J F 2012 *Phys. Rev. E* **85** 056603
[14] Lai X J, Cai X O and Zhang J F 2018 *Commun. Theor. Phys.* **69** 159
[15] Sharma V, Kumar S C, Aadhi A, Ye H, Samanta G K and Ebrahim-Zadeh M 2019 *Sci. Rep.* **9** 9578
[16] Srinivas P, Perumangatt C, Lal N, Singh R P and Srinivasan B 2018 *Opt. Lett.* **43** 2579
[17] Wang R, He S S, Chen S Z, Zhang J, Shu W X, Luo H L and Wen S C 2018 *Opt. Lett.* **43** 3570
[18] Zhang H C, Weng Z W and Yuan J 2021 *Opt. Commun.* **492** 126978
[19] Fang P P, He J T, Asgari R, Gao X L and Lin J 2023 *Eur. Phys. J. Plus* **138** 482
[20] Wang Q, Mihalache D, Belic M R, Zeng L W and Lin J 2023 *Opt. Lett.* **48** 747
[21] Geng K L, Zhu B W, Cao Q H, Dai C Q and Wang Y Y 2023 *Nonlinear Dyn.* **111** 16483
[22] Chen Y X and Xiao X 2022 *Nonlinear Dyn.* **109** 2003
[23] Xu J Z, Cao Q H and Dai C Q 2022 *Commun. Theor. Phys.* **74** 075001
[24] Lu P H, Zhang X F and Dai C Q 2022 *Front. Phys.* **17** 42501
[25] Zhao J B, Luan Z T, Zhang P, Dai C Q, Biswasc A, Liu W J and Kudryashove N A 2020 *Optik* **220** 165189
[26] Wen X K, Jiang J H, Liu W and Dai C Q 2023 *Nonlinear Dyn.* **111** 13343
[27] Li P F and Dai C Q 2020 *Ann. Phys. (Berlin)* **532** 2000048
[28] Ghosh P K 2021 *Phys. Lett. A* **402** 127361
[29] Dai C Q and Zhang J F 2020 *Nonlinear Dyn.* **100** 1621